




## Research Article

# Periapical lesion following Cnm-positive *Streptococcus mutans* pulp infection worsens cerebral hemorrhage onset in an SHRSP rat model

Yuri Taniguchi<sup>1</sup>, Kazuhisa Ouhara<sup>1,\*</sup> , Masae Kitagawa<sup>2</sup>, Keiichi Akutagawa<sup>3</sup>, Miki Kawada-Matsuo<sup>4</sup>, Tetsuya Tamura<sup>1</sup>, Ruoqi Zhai<sup>1</sup>, Yuta Hamamoto<sup>1</sup>, Mikihiro Kajiya<sup>1,5</sup>, Shinji Matsuda<sup>1</sup>, Hirofumi Maruyama<sup>6</sup>, Hitoshi Komatsuzawa<sup>4</sup>, Hideki Shiba<sup>2,3</sup>, Noriyoshi Mizuno<sup>1</sup>

<sup>1</sup>Department of Periodontal Medicine, Graduate School of Biomedical and Health Sciences, Hiroshima University, 1-2-3 Kasumi, Minami-ku, Hiroshima 734-8553, Japan

<sup>2</sup>Center of Oral Clinical Examination, Hiroshima University Hospital, 1-2-3 Kasumi, Minami-ku, Hiroshima 734-8553, Japan

<sup>3</sup>Department of Biological Endodontics, Graduate School of Biomedical and Health Sciences, Hiroshima University, 1-2-3 Kasumi, Minami-ku, Hiroshima 734-8553, Japan

<sup>4</sup>Department of Bacteriology, Graduate School of Biomedical and Health Sciences, Hiroshima University, 1-2-3 Kasumi, Minami-ku, Hiroshima 734-8553, Japan

<sup>5</sup>Department of Innovation and Precision Dentistry, Graduate School of Biomedical and Health Sciences, Hiroshima University, 1-2-3 Kasumi, Minami-ku, Hiroshima 734-8553, Japan

<sup>6</sup>Department of Clinical Neuroscience and Therapeutics, Graduate School of Biomedical and Health Sciences, Hiroshima University, 1-2-3 Kasumi, Minami-ku, Hiroshima 734-8553, Japan

\*Correspondence: Kazuhisa Ouhara, Department of Periodontal Medicine, Graduate School of Biomedical and Health Sciences, Hiroshima University, 1-2-3 Kasumi, Minami-ku, Hiroshima, Japan. Email: [kouhara@hiroshima-u.ac.jp](mailto:kouhara@hiroshima-u.ac.jp)

## Abstract

Cerebral hemorrhage severely affects the daily life of affected individuals. *Streptococcus mutans* and its adhesion factor Cnm increase the adverse effects of cerebral hemorrhages. However, the mechanism by which Cnm-positive bacteria migrate from apical lesions to cerebral hemorrhage sites is unclear. Therefore, we established an *S. mutans*-infected apical lesion in a rat model of hypertension and investigated the neurological symptoms associated with cerebral hemorrhage. Eighteen 12-week-old stroke-prone spontaneously hypertensive rats were randomly divided into three groups, i.e. the no infection (control), dental infection with *S. mutans* KSM153 wild type (Cnm positive), and KSM153  $\Delta$ cnm groups. Immunofluorescent staining was performed to visualize *S. mutans* protein. Serum interleukin-1 $\beta$  levels were measured. The adhesion of *S. mutans* to the extracellular matrix and human fibroblast cells was also analyzed. Serum antibody titers against *S. mutans* were comparable between Cnm positive and knockout mutants. However, 3–10 days post-infection, neurological symptom scores and cerebral hemorrhage scores were higher in Cnm-positive rats than in knockout mutants. The localization of *S. mutans*-derived protein was observed in the vicinity of disrupted blood vessels. Serum interleukin-1 $\beta$  levels significantly increased post-KSM153 WT infection. Cnm-positive *S. mutans* clinical isolates showed increased adhesion to the extracellular matrix, human dental pulp cells, and human umbilical vein endothelial cells compared with the Cnm-negative *S. mutans* isolates. In conclusion, Cnm-positive bacteria colonize the apical lesion site using the extracellular matrix as a foothold and affect cerebral hemorrhage via the bloodstream.

**Keywords:** *Streptococcus mutans*, Cnm, hemorrhage, bacteremia, type IV collagen

**Abbreviations:** CFU: colony-forming unit; Cnm+: Cnm-positive *S. mutans*; Cnm–: Cnm-negative *S. mutans*; ELISA: enzyme-linked immunosorbent assay; Em: erythromycin; ECM: extracellular matrix; HRP: horseradish peroxidase; HDPCs: human dental pulp cells; HUVECs: human umbilical vein endothelial cells; Ig: immunoglobulin; IL-1 $\beta$ : interleukin-1 $\beta$ ; LAMP: loop-mediated isothermal amplification; PBS: phosphate-buffered saline; PBST: PBS supplemented with 0.05% Tween 20; PCR: polymerase chain reaction; SHRSP: stroke-prone spontaneously hypertensive; TSA: trypticase soy agar.

## Introduction

Stroke is responsible for approximately 9% of all deaths worldwide and is the second leading cause of death after ischemic heart disease. The number of patients affected by stroke is increasing owing to changes in lifestyle and a growing aged population [1]. Stroke is primarily of two types,

i.e. ischemic and hemorrhagic [2]. Ischemic stroke, the most common type of stroke, occurs when the cerebral blood vessels become constricted or blocked by fat deposits that accumulate in the blood vessels and when blood clots pass through the bloodstream and lodge in the blood vessels of the brain. Hemorrhagic stroke occurs when a blood vessel in the

Received 19 April 2022; Revised 6 September 2022; Accepted for publication 11 October 2022

© The Author(s) 2022. Published by Oxford University Press on behalf of the British Society for Immunology.

This is an Open Access article distributed under the terms of the Creative Commons Attribution-NonCommercial License (<https://creativecommons.org/licenses/by-nc/4.0/>), which permits non-commercial re-use, distribution, and reproduction in any medium, provided the original work is properly cited. For commercial re-use, please contact [journals.permissions@oup.com](mailto:journals.permissions@oup.com)

brain leaks or ruptures. Factors related to hemorrhagic stroke include uncontrolled high blood pressure, overtreatment with blood thinners (anticoagulants), bulges at weak spots in the blood vessel walls (aneurysms), trauma (such as a car accident), and protein deposits in the walls of blood vessels that result in wall weakening (cerebral amyloid angiopathy) [3]. Ischemic stroke may also lead to hemorrhagic stroke. Several genetic and environmental risk factors associated with stroke occurrence have been identified [4]. However, other causes and risk factors remain unknown [5–7].

Oral diseases are of two major types, i.e. dental caries and periodontal diseases. Periodontal disease is a chronic infection wherein the tissues around the teeth (gingiva, periodontal ligament, and alveolar bone) are destroyed by periodontal pathogenic bacteria, causing tooth loss [8]. However, it may also be associated with various systemic conditions (such as diabetes, liver disease, kidney disease, rheumatoid arthritis, heart disease, Alzheimer's disease, aspiration pneumonia), local diseases in the oral cavity [9], or earlier events such as premature birth, and low birth weight.

In caries, the caries-causing bacterial infection reaches the pulp tissue (local infection) and spreads to the entire body (systemic infection) via infected peripheral blood mononuclear cells from periapical lesions [10]. *Streptococcus mutans*, one of the major causative pathogens of dental caries, is associated with the progression of systemic conditions, including intracerebral hemorrhage, immunoglobulin (Ig)A nephropathy, and inflammatory bowel disease. Furthermore, a 120-kDa collagen-binding protein Cnm has been identified as an (LPXTG)-anchored cell surface protein [11] that acts as a pathogenic factor of *S. mutans*. Approximately 10–20% of the *S. mutans* express Cnm [12]. Cnm-positive *S. mutans* shows a strong association with cerebral hemorrhage in mice. Previously, in mouse and rat models of cerebral hemorrhage, infection with *S. mutans* was achieved via the carotid artery, resulting in bacteremia [13]. Although the possibility of the spread of *S. mutans* from the oral cavity to the site of cerebral microbleeds has been reported, the path by which bacteria are transmitted from the oral cavity to systemic organs remains unclear [14]. Therefore, in the present study, we hypothesize that *S. mutans* pulp infection could affect the occurrence of cerebral hemorrhage via hematogenous movement. To test this hypothesis, we established an *S. mutans* pulp infection model in stroke-prone spontaneously hypertensive (SHRSP) rats and determined the effect of *S. mutans* infection on the progression of cerebral hemorrhage.

## Materials and methods

### Bacterial strains and construction of *cnm*-knockout mutants

*Streptococcus mutans* was grown in Trypticase soy broth (Becton Dickinson Microbiology Systems, Cockeysville, MD, USA) or Trypticase soy agar (TSA) at 37 °C in the presence of 5% CO<sub>2</sub>. Erythromycin (10 µg/ml) was added when necessary. *cnm* single-deletion mutants (KSM153  $\Delta$ *cnm*) were constructed via overlapping extension polymerase chain reaction (PCR), as described previously [15]. Briefly, to generate the *cnm* deletion mutant, two fragments corresponding to approximately 500 bp of the upstream and downstream sequences of this gene were generated via PCR using KOD Plus (Toyobo, Tokyo, Japan) with primer pairs for the upstream fragment

*cnm*-F1 (forward 5'-CCGTTGCCATCATTTTGC-3', and reverse 5'-CAGTCGAGGATTGCCGCCGCTGGTAA-3') and downstream fragment *cnm*-F2 (forward 5'-GCTGACCTAGTAGAAGCTCCAACAACAAC-3', and reverse 5'-GTCCCTTGGTACCAGC-3'). Each of the F1 reverse and F2 forward primers contained 11 bases complementary to the erythromycin resistance cassette (Em<sup>r</sup>) that were cloned using pBlueScript-Em (StrataGene, La Jolla, CA, USA). The Em<sup>r</sup> gene was amplified via PCR using primers for Em<sup>r</sup>. All PCR amplicons were purified using a PCR purification kit (Qiagen KK, Tokyo, Japan). The corresponding upstream and downstream amplicons were mixed at a 1:1:1 ratio with the Em<sup>r</sup> PCR product. The amplicon mixture was then used as the template for a second PCR using forward *cnm*-F1 and reverse *cnm*-F2 primers. The resulting PCR products were then transformed into *S. mutans*, as described previously [15]. The mutation was verified using PCR.

*Streptococcus mutans* clinical isolates were collected from the saliva of 102 patients who underwent examination of dental caries risk at the Center of Oral Clinical Examination in Hiroshima University Hospital, as shown previously [16]. All experimental protocols were approved by the epidemiological research ethics review committee of Hiroshima University (E-786-2). The detection of Cnm-positive or -negative *S. mutans* was performed by loop-mediated isothermal amplification (LAMP) after culturing in mitis salivarius-bacitracin agar. The recovered *S. mutans* (11 Cnm-positive strains and 24 Cnm-negative strains) were used in this study.

### Dental infection of rats with *S. mutans*

The experimental protocol described below was approved by the Animal Care Committee of Hiroshima University (A18-112). In total, 18 SHRSP rats (12 weeks old, Japan SLC, Inc., Tokyo, Japan) were housed in a climate-controlled (temperature 22–24 °C, humidity 40–60%), light-regulated room under a 12 h light/dark cycle. All rats consumed the general diet (SP diet, CLEA Japan, Inc., Tokyo, Japan). Rats were allowed free access to rat chow and drinking water before the experiment. The animal research adheres to the ARRIVE guidelines. All rats were randomly divided into three groups ( $n = 6$ ), namely, no infection (control) and dental infection with either *S. mutans* (KSM153 WT (Cnm-positive) or KSM153  $\Delta$ *cnm*). For dental infection with *S. mutans*, the roofs of the pulp chambers of the right and left first molars of the lower jaw were removed using a #1/2 round bar [17]. After removing the coronal pulp, a small cotton swab soaked in 10 µl phosphate-buffered saline (PBS) containing 10<sup>8</sup> *S. mutans* cells (10<sup>8</sup> colony-forming units: CFUs) was placed into the pulp chamber and sealed using Caviton (GC Co., Tokyo, Japan). Meanwhile, the rats were bred with rat chow containing 2% NaCl and drinking water containing 2% NaCl for inducing cerebral hemorrhage [18]. After 10 days of *S. mutans* infection, tissue samples were taken from the lower jaw for the detection of *S. mutans* and micro-computed tomography (CT) analysis and from the brain for histological evaluation. Sera were also collected and stored at –80 °C prior to determining the IgG titer against *S. mutans* and the IL-1 $\beta$  levels.

### Micro-CT analysis

In the micro-CT analysis, rats were scanned using the Skyscan 1076 system (Bruker, Kontich, Belgium) to evaluate

bone destruction at the periapical site. The joint samples were scanned and reconstructed at 18  $\mu\text{m}^3$  voxels using the micro-CT system [19].

### Analysis of neurological deficit

Forelimb and hindlimb flexion, forelimb motor function, postural reaction, and the posture of each animal were monitored every 3 days. The items considered in the neuronal deficit and judgment are mentioned below. Animals were placed on a large rubber sheet that could be gripped firmly by their claws to assess the postural reaction. Gentle lateral pressure was applied behind the animal's shoulder until it slid about 15 cm. Each item was scored 0–3 (0: the animal resisted sliding equally in both directions; 1: resistance to lateral push toward the right was slightly reduced; 2: resistance to lateral push toward the right was markedly reduced; 3: resistance to lateral push toward the right was markedly reduced, and the animal fell on its back) [20], and the animal with the most severe symptoms was scored 15 points. The bleeding score was calculated as the sum of the number of  $\geq 1$  mm bleeding spots in the central frontal section of each rat brain. The blood vessel score for dilated blood vessels was calculated as the sum of the number of blood vessels with a diameter  $\geq 20$   $\mu\text{m}$  in the section (2.2 mm  $\times$  3.0 mm) of each rat brain.

### Detection of interleukin (IL)-1 $\beta$ in rat serum

Serum IL-1 $\beta$  levels were measured using a rat IL-1 $\beta$  enzyme-linked immunosorbent assay (ELISA) kit (ab100767, Abcam, Tokyo, Japan), following a published protocol [21]. Briefly, the sera were diluted four times with PBS. A solid-phase anti-IL-1 $\beta$  monoclonal antibody was diluted to a final concentration of 1  $\mu\text{g}/\text{ml}$  in coating buffer and was then applied to a 96-well ELISA plate (BD Falcon, Franklin Lakes, NJ, USA) for target capture. Each well was subsequently blocked with 1% BSA in PBS supplemented with 0.05% Tween 20 (PBST), and the sample or standard (diluted from 1 ng/ml to zero in PBST) was applied to each well. After adding the detection antibody (diluted to a final concentration of 1  $\mu\text{g}/\text{ml}$  in PBST), horseradish peroxidase (HRP) conjugated with anti-IgG (2000-fold dilution in PBST) was applied to the wells. Colorimetric reactions were developed with o-phenylenediamine (Sigma-Aldrich) in the presence of 0.02%  $\text{H}_2\text{O}_2$ . Color development was halted using  $\text{H}_2\text{SO}_4$  (2N) and measured using an ELISA reader (OD<sub>405</sub>, Varioskan LUX). The actual concentration of the target was calibrated by comparing it to a standard curve prepared from serial dilutions. Each sample was analyzed in triplicate wells of the 96-well ELISA plate. The limit of rat IL-1 $\beta$  detection for each analyte was 4.3 pg/ml.

### Cell culture

Human dental pulp cells (HDPCs) were purchased from Lonza (Walkersville, MD, USA) and cryopreserved at passage 3. HDPCs were sub-cultured in  $\alpha$ -Minimum Essential Medium (Thermo Fisher Scientific, Tokyo, Japan) supplemented with 10% fetal bovine serum (FBS) and 100 U penicillin/streptomycin at 37 °C in humidified air with 5%  $\text{CO}_2$ . Human umbilical vein endothelial cells (HUVECs) were purchased from Cambrex Bio Science Walkersville, Inc. (Walkersville, MD, USA). They were maintained in EBM-2 medium (Lonza) supplemented with FBS, fibroblast growth factor, epidermal endothelial growth factor, hydrocortisone,

insulin-like growth factor, ascorbic acid, vascular epithelial growth factor, and amphotericin B. Human gingival fibroblasts (HGFs) were purchased from the American Type Culture Collection (ATCC, Manassas, VA, USA) and cryopreserved at passage 3. HGFs were sub-cultured in Dulbecco's Modified Eagle Medium (Thermo Fisher Scientific, Tokyo, Japan) supplemented with HDPCs.

### Western blot analysis

Western blotting was conducted to confirm the production of extracellular matrix (ECM) in HDPCs, HUVECs, and HGFs. The cultured cells were lysed using 100  $\mu\text{L}$  of 1 $\times$  lysis buffer (Thermo Fisher Scientific) containing a 1% proteinase inhibitor cocktail (87786, Thermo Fisher Scientific) and 0.1% phenylmethanesulfonyl fluoride (Fluka, BioChemika, Tokyo, Japan). The samples were electrophoresed on a 10% sodium dodecyl sulfate-polyacrylamide gel and then electrically transferred onto nitrocellulose membranes (BioRad Laboratories, Hercules, CA, USA). The nitrocellulose membranes were blocked with 1% nonfat dried milk at 25 °C for 1 h, followed by a reaction with anti-type I collagen monoclonal IgG (10  $\mu\text{g}/\text{ml}$ ; NB600-408, Novus Biologicals), anti-type IV collagen monoclonal IgG (10  $\mu\text{g}/\text{ml}$ ; ab6586, Abcam), anti-laminin monoclonal IgG (10  $\mu\text{g}/\text{ml}$ ; sc-74531, Santa Cruz Biotechnology, Inc.), or anti-fibronectin monoclonal IgG (10  $\mu\text{g}/\text{ml}$ ; sc-8422, Santa Cruz Biotechnology, Inc.) in PBS-Tween 20 at 4 °C for 12 h. The anti-vimentin monoclonal antibody (10  $\mu\text{g}/\text{ml}$ ; sc-6260, Santa Cruz Biotechnology, Inc.) was used as an internal control. Membranes were incubated with horseradish peroxidase-conjugated sheep anti-mouse IgG in PBS-Tween 20 at 25 °C for 1 h. Immunodetection was conducted according to the instructions of the ECL Plus Western Blotting kit (GE Healthcare Life Sciences, Osaka, Japan) [22].

### Detection of *S. mutans* in rat tissue

After collecting rat serum, periapical tissue, and brain tissue, DNA was extracted from the samples using the DNeasy Blood and Tissue kit (Qiagen KK). To identify the *S. mutans* strain, *gtf* was amplified using PCR [16] and the following primers: forward 5'-GGCACCACAACATTGGGAAGCTCA GTT-3' and reverse 5'-GGAATGGCCGCTAAGTCAACAGG AT-3'. To detect *S. mutans* in the periapical region, western blotting was conducted using anti-*S. mutans* serum purified from an *S. mutans*-immunized mouse. The *S. mutans* LM-7 strain was used as the positive control.

### Histology of rat brain tissue

Brain tissues were fixed in 4% buffered formalin and embedded in paraffin wax. The paraffin-embedded tissues were then sliced into 5  $\mu\text{m}$  sections, mounted on glass slides, and stained with hematoxylin and eosin (H&E) to detect microvasculature disruption. *S. mutans* localization in the brain tissues was visualized using immunohistochemistry. *S. mutans* was detected using anti-*S. mutans* mouse IgG (10  $\mu\text{g}/\text{ml}$ ) for 30 min at 25 degrees followed by fluorescein isothiocyanate (FITC)-labeled anti-mouse IgG (Jackson ImmunoResearch, West Grove, PA, USA). The nucleus was stained with Dapi-Fluoromount G (Southern Biotech Inc., Birmingham, AL, USA). Section signals were detected using

a fluorescence microscope (model BZ-9000; Keyence, Osaka, Japan).

### Adhesion and invasion of *S. mutans* to ECM

An overnight culture of *S. mutans* was pelleted via centrifugation ( $3000 \times g$  for 10 min). The pellet was then washed and resuspended in PBS. The bacterial suspension was adjusted to a density of  $10^8$  bacterial cells/ml, and 100  $\mu$ l of the suspension was spread over ECM-precoated 96-well plates (type I collagen, #356407; type IV collagen, #354429; laminin, #354410; fibronectin, #354409; all from Corning) or seeded in 96-well plates containing HDPC or HUVEC cultures ( $10^7$  cells for investigating adhesion to ECM-precoated plates,  $10^5$  cells for investigating adhesion to HDPCs, HUVECs, or HGFs), and incubated for 3 h in the presence of antibiotic/FBS-free medium. For the adhesion assays, the samples cultured in 96-well plates were washed thrice with PBS, following which 0.25% trypsin was added to remove the adherent bacterial cells from the plastic dish. For invasion assays, the samples cultured in 96-well plates were incubated for 1 h with gentamycin (300  $\mu$ g/ml) for 1.5 h before adding 0.25% trypsin, as in the adhesion assay. After adding 100  $\mu$ l PBS, the bacterial suspension was diluted appropriately, plated on TSA, and incubated for 3 days at 37 °C. Colonies were counted as adhesive or invading bacterial cells [23].

### Knockdown of ECM by siRNA transfection

The mRNA expression of type I collagen, type IV collagen, laminin, and fibronectin was suppressed by transfection of specific siRNA (type I collagen, type IV collagen, laminin, and fibronectin, Sigma-Aldrich). Briefly, HUVECs and HDPCs were cultured until 70% confluency at the time of transfection in the 6-well plate. Lipofectamine RNAiMax (6  $\mu$ L, Invitrogen, Tokyo, Japan) was then diluted into 100  $\mu$ L of medium without supplements. The mixture was added into cell culture following the addition of siRNA (final concentration: 10 nM) into the reagents. As a negative control, siRNA Universal Negative Control #1 (#SIC001-10NMOL, Sigma-Aldrich) was transfected into cells using the same protocol. The suppression of mRNA was detected in 6 h by real-time PCR using specific primers as shown Table S1. PCR protocol was shown previously [22]. The knockdown of target proteins was also confirmed using western blotting within 12 h.

### Statistical analysis

All experiments were independently performed at least three times. Shapiro–Wilk tests for distribution normality were conducted for each data set. Data are expressed as mean  $\pm$  standard deviation. Comparisons between two groups were performed using a two-tailed unpaired Student's *t*-test or Mann–Whitney *U* test (for non-normal distributions). For multiple comparisons, one-way ANOVA with Tukey–Kramer post hoc tests was used.  $P < 0.05$  was considered significant.

## Results

### Infection of rat tooth pulp with *S. mutans*

A micro-CT image showed apical lesions in SHRSP rats with dental pulp KSM153 WT or KSM153  $\Delta$ *cnm* *S. mutans* infection (Fig. 1A). In contrast, rats without *S. mutans* infection did not show apical bone resorption. *S. mutans* infection was confirmed by elevated serum IgG titers against *S. mutans* using

ELISA (WT:  $64.9 \pm 21.1\%$  increase;  $\Delta$ *cnm*:  $61.62 \pm 27.9\%$  increase) (Fig. 1B). *S. mutans* systemic infection was also confirmed by detection of *S. mutans* *gtf* DNA using PCR. The target DNA was amplified from the serum of both the KSM153 WT- and KSM153  $\Delta$ *cnm*-infected groups (Fig. 1C). Western blotting was conducted to detect *S. mutans* colonies in the periapical lesions. *S. mutans* protein was detected in the periapical tissue of KSM153 WT- and KSM153  $\Delta$ *cnm*-infected rats using anti-*S. mutans* WT-immunized mouse IgG (Fig. 1D).

### Analysis of cerebral hemorrhage in rats

The brain of the rat model of cerebral hemorrhage was dissected sagittally, and the presence or absence of bleeding was assessed (Fig. 2A). The H&E-stained brain sections in the KSM153 WT-infected group showed an increased number of dilated blood vessels as well as vessel wall disruption (Fig. 2A and C). Furthermore, *S. mutans*-derived protein was localized in the walls of disrupted blood vessels in sections of the KSM153 WT-infected group (Fig. 2A). The bleeding scores of KSM153 WT-infected rats ( $29.2 \pm 3.1$ ) were significantly higher than those of control (Ctrl;  $13.5 \pm 3.5$ ) and KSM153  $\Delta$ *cnm*-infected ( $12.6 \pm 6.8$ ) rats (Fig. 2B). In addition, the number of dilated blood vessels ( $\geq 20 \mu$ m) in KSM153 WT-infected rats ( $13.0 \pm 1.8$ ) were significantly higher than those in control (Ctrl;  $7.0 \pm 1.2$ ) and KSM153  $\Delta$ *cnm*-infected ( $9.0 \pm 1.2$ ) rats (Fig. 2C). Next, the neurological score was determined. As shown in Fig. 2D, the neurological scores of the Ctrl group did not change after 10 days ( $0 \pm 0$ ). However, the neurological scores of the KSM153 WT- and KSM153  $\Delta$ *cnm*-infected groups increased over time (Fig. 2D). In addition, the neurological scores of the KSM153 WT-infected group ( $4.2 \pm 1.1$ ) were significantly higher than those of the KSM153  $\Delta$ *cnm*-infected group ( $1.0 \pm 0.7$ ) 10 days post-infection (Fig. 2D). The number of hemorrhagic spots in the brain tissue of the KSM153 WT-infected group increased after infection.

### IL-1 $\beta$ production in the serum and brain tissue

The serum level of IL-1 $\beta$  was measured using ELISA to assess the inflammatory response. The IL-1 $\beta$  level in the KSM153 WT-infected group ( $33.3 \pm 8.7$  pg/ml) was significantly higher than those of the Ctrl ( $15.6 \pm 7.7$  pg/ml) and KSM153  $\Delta$ *cnm*-infected ( $16.2 \pm 7.4$  pg/ml) groups (Fig. 2E).

### Adhesion of *S. mutans* to HUVECs, HDPCs, HGFs, and the ECM

We assayed the adhesion of *S. mutans* to the ECM and ECM-producing cells (HDPCs, HUVECs, and HGFs), as adhesion is a trigger for *S. mutans* tissue infection. Before the adhesion assay, we confirmed the production of four types of ECM (type I collagen, type IV collagen, laminin, and fibronectin) by HDPCs, HUVECs, and HGFs using western blotting (Fig. 3A). Next, the adhesion of *S. mutans* KSM153 WT and KSM153  $\Delta$ *cnm* to HDPCs, HUVECs, HGFs, and the ECM was assessed. The numbers of KSM153  $\Delta$ *cnm* cells that adhered to type I collagen- (56.9%), type IV collagen- (67.2%), and laminin-coated (86.9%) plates were lower than those of KSM153 WT cells (Fig. 3B–D). However, the adhesion of KSM153 WT to fibronectin did not differ from that of KSM153  $\Delta$ *cnm* (Fig. 3E). The number of KSM153  $\Delta$ *cnm* cells adhering to HDPCs (66.9%), HUVECs (62.4%), HGFs (48.5%) was significantly lower than that of KSM153 WT

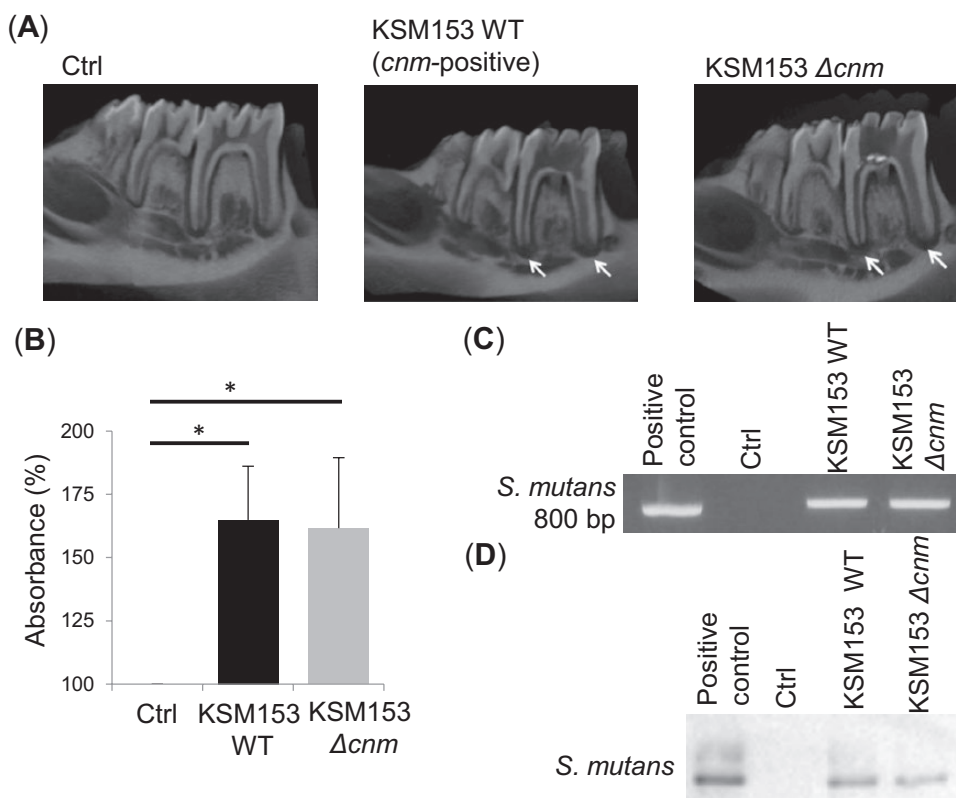


**Figure 1:** effects of *Streptococcus mutans* infection on the periapical lesion of stroke-prone spontaneously hypertensive rats. (A) Pulp tissue of the right and left mandibular first molar teeth of rats (12-week old,  $n = 6$  per group) was infected with live *S. mutans* ( $10^8$  bacteria/rat). Periapical lesions in rat mandibular jaws are indicated by arrows. (B) Levels of serum immunoglobulin (Ig) G against *S. mutans* in rats ( $n = 6$ /group) sacrificed on day 10 were measured using enzyme-linked immunosorbent assay. The ratio of each IgG is shown. \* $P < 0.01$  compared with the control group; one-way ANOVA with Tukey–Kramer post-hoc. (C) *S. mutans*-specific *gtf* DNA in serum amplified using polymerase chain reaction. (D) *S. mutans*-derived protein in periapical lesion detected using western blotting. The representative sample of each group was determined. Chromosomal DNA and lysates of the *S. mutans* LM-7 strain were used as positive controls. Ctrl, control; KSM153 WT, Cnm-positive KSM153.

(Fig. 3F–H). An invasion assay in HUVECs was performed to identify any additional functions of Cnm. The number of KSM153  $\Delta cnm$  cells that invaded HUVECs was inhibited by 99.2% compared with the number of KSM153 WT cells (Fig. 3I).

To determine the specificity of Cnm binding to ECM, siRNA to type I collagen, type IV collagen, laminin, and fibronectin was transfected and confirmed the mRNA expression and protein production in HDPCs and HUVEC. The knockdown of four different ECMs was confirmed as shown in Fig. 4A–H. In this condition, the adhesion of KSM153 WT to type I collagen and type IV collagen was statistically decreased in HDPCs and HUVECs, respectively. The binding of HDPCs and HUVECs to cells with laminin knockdown was not affected due to the continued dominance of type I collagen and type IV collagen expression. The binding to fibronectin knockdown cells did not show any difference in HDPCs and HUVECs (Fig. 4I and J).

The localization of types I and IV collagen in layered tissues, such as the epithelium and blood vessels, differs. Type IV collagen is strongly expressed in the basal lamina and is exposed when blood vessels are disrupted [24]. Therefore, the adhesion of 35 clinical isolates [11 Cnm-positive *S. mutans* (Cnm+) and 24 Cnm-negative *S. mutans* (Cnm–)] to type IV collagen and HUVECs was assessed. The Cnm+ group adhered significantly more to type IV collagen than the Cnm– group (60.5% less adhesion) (Fig. 5A). Cnm+ clinical isolates attached more to HUVECs than the Cnm– ones (76.8% less

adhesion) (Fig. 5B). The invasion rate of Cnm+ clinical isolates to HUVECs was also higher than that of Cnm– ones (94.9% less invasion) (Fig. 5C).

## Discussion

This study showed that *S. mutans* pulp infection promoted microbleeding in the brain of a rat model of cerebral hemorrhage. In particular, the Cnm-positive strain, which produces an *S. mutans* surface protein, strongly affected neurological symptoms owing to cerebral hemorrhage. Furthermore, Cnm-positive *S. mutans*-derived protein was localized in disrupted vessel walls in the rat model. The mechanism via which *S. mutans* colonizes the brain appeared to be associated with bacterial attachment to the ECM, namely, type I collagen, type IV collagen, and laminin.

As a major etiological factor of dental caries, the virulence of *S. mutans* is mainly caused by its ability to form biofilms (dental plaque) on tooth surfaces, generate large amounts of lactic acid, and resist adverse environmental conditions such as low pH and oxidative stresses [25]. Its ability to form strong biofilms potentially leads to enamel demineralization and the establishment of firmly bound biofilms that are difficult to remove from the tooth surface [26]. Therefore, *S. mutans* colonization results in caries development, which may cause endodontic infections if left untreated. In addition, the increase in binding activity by collagen-binding proteins,

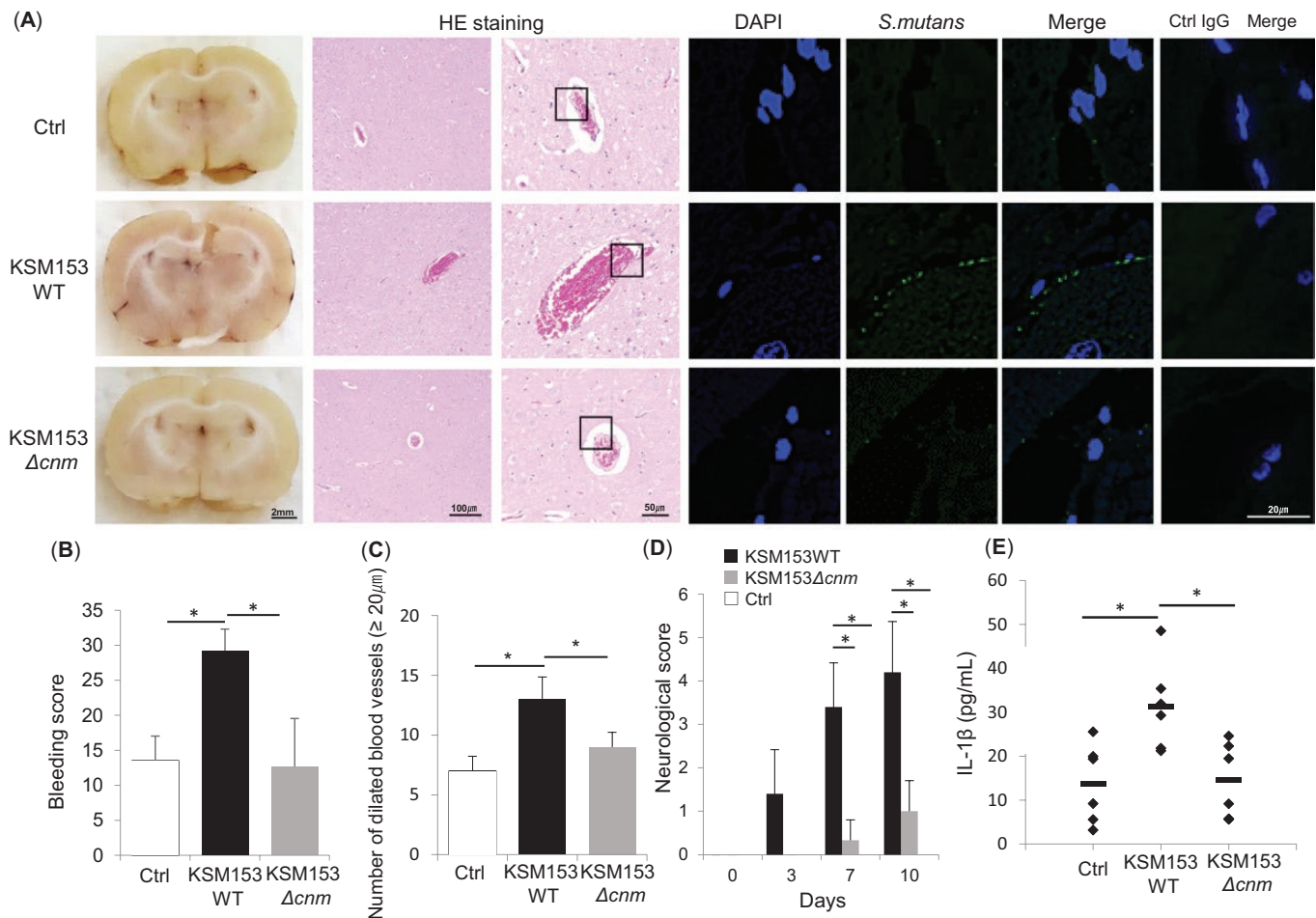


**Figure 2:** effects of *Streptococcus mutans* infection on the brain tissue of stroke-prone spontaneously hypertensive rats. (A–C) Pulp tissue of the right and left mandibular first molar teeth of rats was infected with live *S. mutans*. Rats of all groups were sacrificed 10 days later, brain tissue was collected, and the bleeding score was calculated based on the gross findings of the sagittal section. Blood vessel score for dilated blood vessels was also calculated using H&E-stained sections. Immunofluorescent staining was performed to visualize *S. mutans*-derived protein by anti-Sm IgG-FITC. Nuclei were counter-stained with DAPI. \* $P < 0.01$ ; one-way analysis of variance (ANOVA) with Tukey–Kramer post-hoc. (D) Neuronal deficit (forelimb and hindlimb flexion, forelimb motor function, postural reaction, and posture) of rats in the three groups was assessed on days 0, 3, 7, and 10. \* $P < 0.01$ ; one-way ANOVA with Tukey–Kramer post-hoc. (E) Interleukin (IL)-1 $\beta$  level in serum isolated from rats sacrificed on day 10 ( $n = 6$ /group) was measured using enzyme-linked immunosorbent assay. \* $P < 0.01$ ; one-way ANOVA with Tukey–Kramer post hoc. Ctrl, control; KSM153 WT, Cnm-positive KSM153, KSM153  $\Delta cnm$ , Cnm-knockout mutant.

such as Cnm, appears to promote biofilm accumulation and tight binding to collagenous surfaces such as root canals [27]. As a human pathogen, *S. mutans* is also implicated in sub-acute bacterial endocarditis, a life-threatening inflammation of the cardiac valves. Some strains of *S. mutans* have also been associated with other extraoral pathologies such as cerebral microbleeding, IgA nephropathy, and atherosclerosis [25]. Cnm is a type I collagen-binding protein, and infection of the carotid artery in mice and rats by *S. mutans* causes cerebral hemorrhage. Epidemiologically, as an indigenous bacterium of the oral cavity, Cnm-positive *S. mutans* is known to cause the onset of cerebral hemorrhage (double the odds ratio) [28].

In previous studies, *S. mutans* infection occurring in the blood vessels, carotid artery, or near the brain allowed us to easily perceive the direct effect of *S. mutans* on cerebral hemorrhage [13]. However, in this study, *S. mutans* physiologically colonized the oral cavity of rats, and, hence, understanding its effects on distant organs, such as the brain, was challenging. *S. mutans* colonizes the oral cavity in the form of plaque/biofilm on the tooth surface and infects the pulp by

decalcifying the tooth with acid. Here, we clarified that Cnm also affects *S. mutans* attachment to dental pulp cells via its adhesion to the ECM. During the infection of dental pulp cells, *S. mutans* Cnm was involved in strongly binding to not only type I collagen but also type IV collagen and laminin. Moreover, the micro-CT analysis revealed a similar scenario in the apex of teeth infected with Cnm-positive and -negative *S. mutans* strains. However, Cnm, which strongly adheres to tissues, also increased serum IL-1 $\beta$  production, suggesting that bacterial colonization in periapical lesions can sustainably maintain bacteremia and is the first step toward systemic infection via bacteremia.

*S. mutans* affects the outcome of various diseases owing to the associated bacteremia, during which *S. mutans* is transferred from the apical lesions to the whole body. Collagen-binding proteins produced by *S. mutans*, such as Cnm, may inhibit platelet aggregation and cause bleeding [13]. Cnm can interrupt the interaction between exposed collagen fibers on damaged endothelium and platelet surfaces, thereby effectively disrupting the initiation of platelet aggregation and

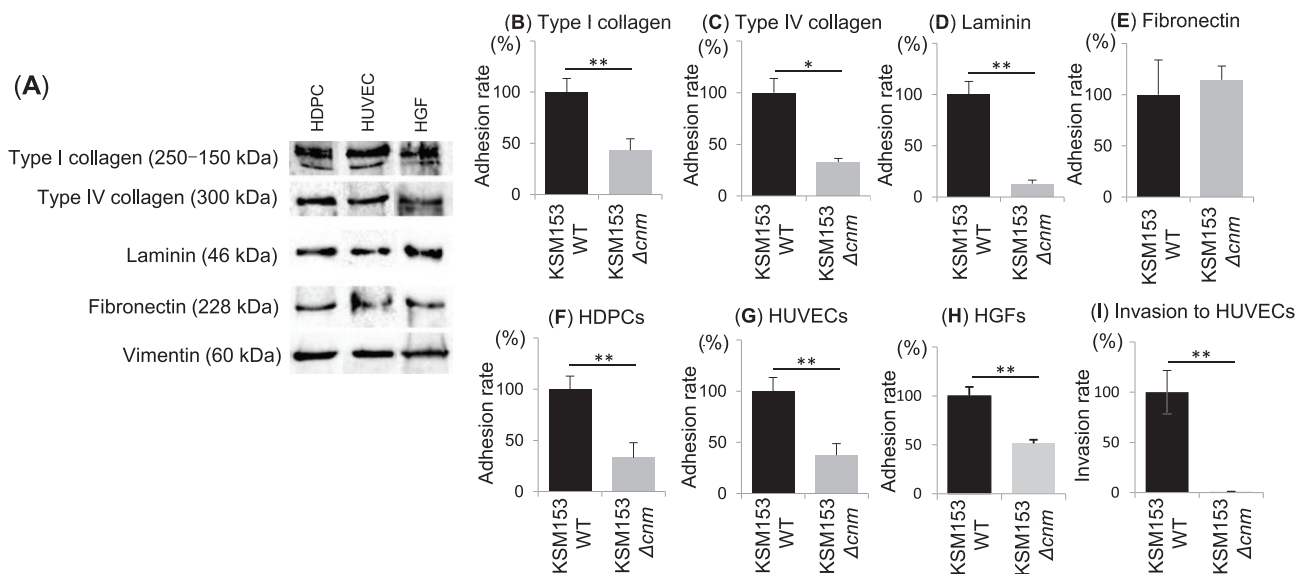


**Figure 3:** Adhesion of *Streptococcus mutans* to the extracellular matrix (ECM), human dental pulp cells (HDPCs), human umbilical vein endothelial cells (HUVECs), and human gingival fibroblasts (HGFs): (A) Expression of ECM components (type I collagen, type IV collagen, laminin, and fibronectin) in HDPCs, HUVECs, and HGFs assessed using western blotting. Vimentin was used as the positive control. (B–G) Adhesion of *S. mutans* to (B–E) ECM components, (F) HDPCs, (G) HUVECs, and (H) HGFs. (I) Invasion of *S. mutans* to HUVECs. *S. mutans* ( $10^6$  bacterial cells/ml, 100  $\mu$ l of suspension ( $10^7$  cells)) was applied to 96-well plates and cultured for 3 h. Cells were washed for adhesion assay and for invasion assay, were incubated for 1 h with gentamycin (300  $\mu$ g/ml) for 1.5 h, 0.25% trypsin was added to remove adherent bacterial cells, and the bacterial suspension was plated on TSA and incubated for 2 days at 37  $^{\circ}$ C. Colonies were counted as total cell number, including adhesive cells. \* $P < 0.01$ , \*\* $P < 0.001$ ; Student's *t*-test. Ctrl, control; KSM153 WT, Cnm-positive KSM153, KSM153  $\Delta cnm$ , Cnm-knockout mutant.

inhibiting hemostasis. Furthermore, Cnm-positive *S. mutans* activates matrix metalloproteinases, which leads to further disruption of blood vessel barriers and bleeding [13, 29]. Therefore, not only type I collagen but also type IV collagen, which is located closer to the basal layer and is exposed by the destruction of the blood vessel wall, are targeted by *S. mutans* at the site of a cerebral hemorrhage. Indeed, in the comparative analysis of *S. mutans* adhesion to type IV collagen in this study, the Cnm-positive strain and clinical isolates adhered better than the Cnm-negative ones.

In a previous study,  $1 \times 10^9$  CFU *S. mutans* were injected into 6-week-old specific-pathogen-free Sprague–Dawley rats via the jugular vein. Then, *S. mutans*-derived DNA was purified and amplified using PCR. *S. mutans* was detected in the blood after 72–120 h [30]. Interestingly, in this study, *S. mutans*-derived DNA was detected in the serum only 10 days after dental pulp infection. As apical lesions were observed in CT images of both the WT and  $\Delta cnm$  *S. mutans*-infected groups, and as the *S. mutans*-derived protein was also detected in the lesion, we concluded that periapical lesions were a continuous source of *S. mutans*, resulting in cerebral hemorrhage owing to long-term bacteremia. However, the size of the apical lesions formed by KSM153 WT and KSM153  $\Delta cnm$  did not differ. In addition, the protein pattern of *S. mutans* detected in the periapical lesions of rats infected with either strain did not vary. Collectively, Cnm does not appear to strongly affect infection in the apical tissues of the jaw. This is because *S. mutans* possesses other molecules, such as gtf, gbp, GP340, DMBT-a, AgI/II, P1, and WapA, that enable it to colonize the pulp and periapical tissue in the oral cavity (source of infection) in the absence of Cnm [31, 32]. As evidence, when the adhesion of *S. mutans* to HGFs was examined, the reduction rate of KSM153  $\Delta cnm$  strain was lower than that of HUVEC and HDPC compared with the adhesion

of KSM153 WT strain. In contrast, a strong adhesion factor is required for adhesion to systemic organs when *S. mutans* disseminates in the body; our observations indicate that Cnm acts as a strong adhesion molecule in the brain.

The detection of *S. mutans*-derived protein in disrupted vessel walls might support the hypothesis of the physiological effect of Cnm in the progression of cerebral hemorrhage (Fig. 2). The neurological symptoms differed between the KSM153 WT and KSM153  $\Delta cnm$ -infected groups. This might have been due to the action of Cnm as an attachment factor as well as the local elevation in the levels of matrix metalloproteinase 9 and inflammatory cytokines as a result of the immune response to bacterial infection. However, alive bacteria were not recovered by culture tests. The antibody used in this study was a polyclonal antibody against *S. mutans* whole cell. Therefore, a positive signal in the stained image may be components derived from bacteria. A potential limitation of this study is the uncertainty regarding the mechanism behind the pathological effect of Cnm in cerebral hemorrhage and in inducing neurological symptoms. It might be due to either the infection and growth of *S. mutans* or the activation of the immune response by the bacterial component of *S. mutans*. The number of *S. mutans* cells ( $10^8$  CFU) used to induce the dental infection is clinically relevant. However, fewer numbers of cells might realistically be sufficient to cause an infection in human patients. Disruption of the blood–brain barrier (BBB) formed by endothelial cells, astrocyte, and pericytes embedded is thought to be necessary for *S. mutans* to colonize sites of cerebral hemorrhage. It has been reported that pneumococci invade the BBB via platelet-activating factor receptor (PAFR). Adherence to polymeric immunoglobulin receptor (pIgR) and platelet endothelial cell adhesion molecule (PECAM-1, CD31) via the key adhesins pneumococcal pilus-1, RrgA also influences brain infection [33]. In this study, the

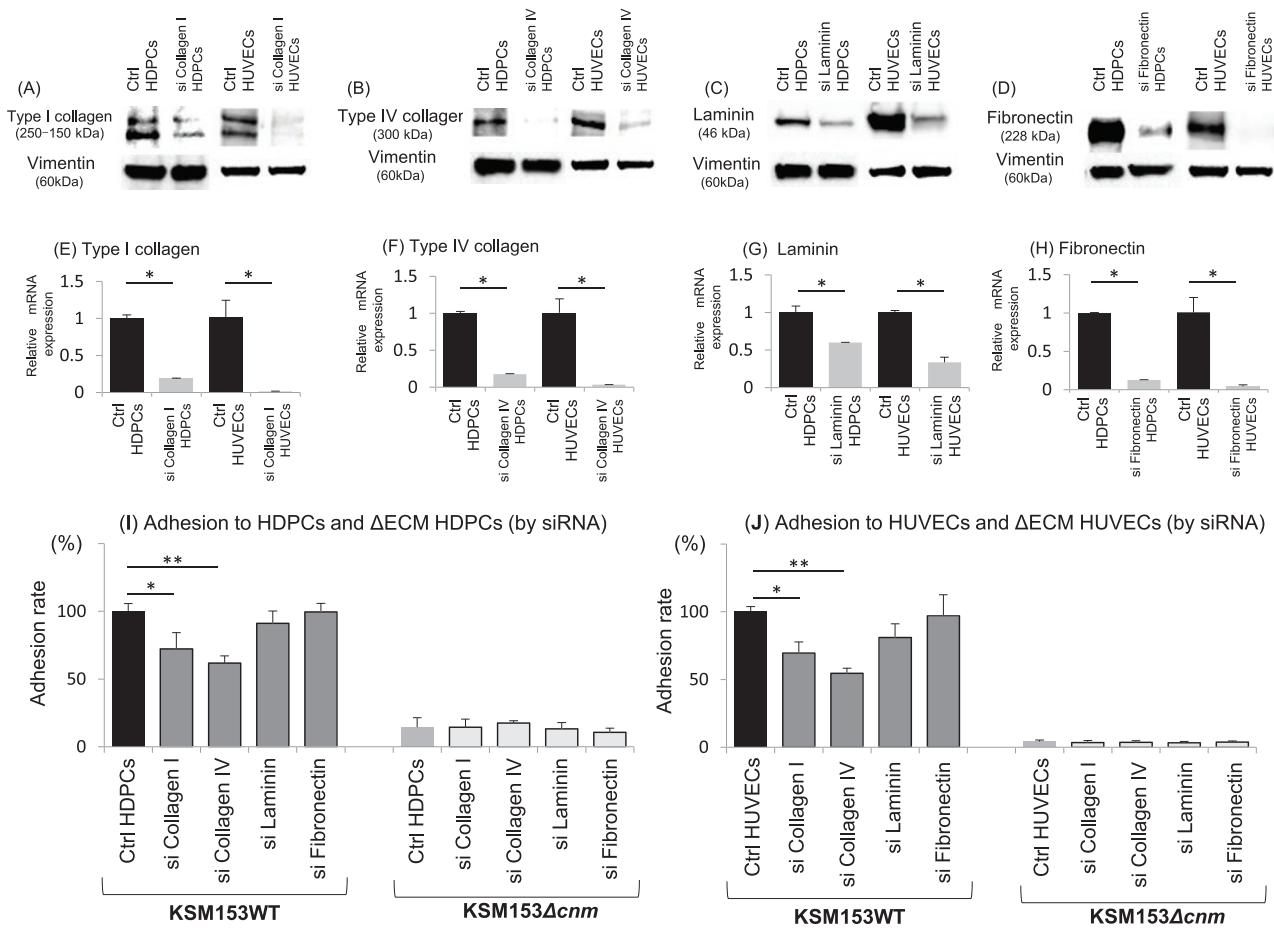


**Figure 4:** adhesion of *Streptococcus mutans* to human dental pulp cells (HDPCs) and human umbilical vein endothelial cells (HUVECs). (A–H) Expression of ECM components (type I collagen, type IV collagen, laminin, and fibronectin) after transfection of specific siRNA in HDPCs and HUVECs assessed using western blotting (A–D) and real-time PCR (E–H). Adhesion of *S. mutans* to (I) HDPCs and (J) HUVECs after transfection of specific siRNA against ECMs. Colonies were counted as total cell number, including adhesive cells. \* $P < 0.01$ , \*\* $P < 0.001$ ; Student's *t*-test. KSM153 WT, Cnm-positive KSM153, KSM153  $\Delta$ cnm, Cnm-knockout mutant.

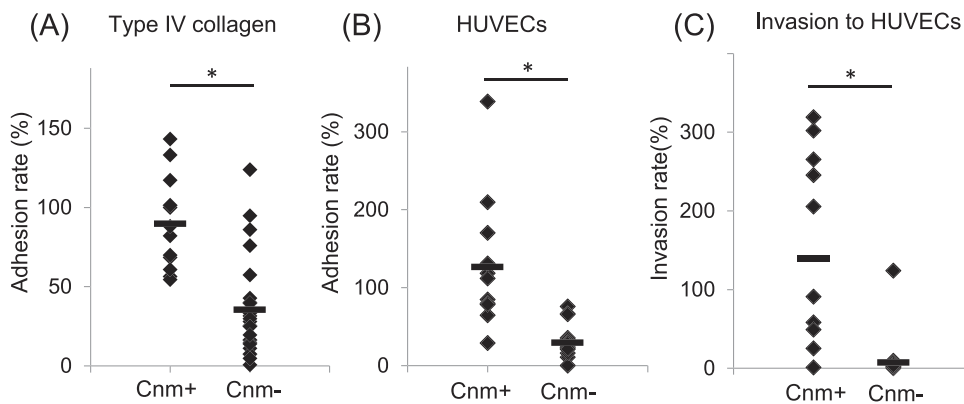


**Figure 5:** adhesion of *Streptococcus mutans* clinical isolates to type IV collagen and human umbilical vein endothelial cells (HUVECs). Graphs show the rate of adhesion of each strain relative to that of LM-7 adherent cells. \* $P < 0.01$ ; Mann–Whitney *U* test. Cnm+, Cnm-positive *S. mutans* clinical isolates; Cnm–, Cnm-negative *S. mutans* clinical isolates.

localization of CD31 in the site of disrupted blood vessels of the KSM153 WT-infected group was not detected because of the destruction of tight junctions, adherence junctions, and CD31, which are important components of the BBB [34, 35]. Further brain tissue analysis is required for complete elucidation of this phenomenon.

In conclusion, the present study shows the involvement of Cnm-positive *S. mutans* in the exacerbation of cerebral hemorrhage in a rat model. This might be mediated by the *S. mutans* attachment to type IV collagen. However, whether vaccines aimed at suppressing caries target antigens on the surface of *S. mutans* remains unclear. It is possible that host



tolerance to *S. mutans* allows the colonization of the oral cavity by this pathogen. However, even small amounts of *S. mutans* can be virulent when spread to the entire body and may affect the pathology of various systemic diseases. In the future, aggravation of these diseases can be halted, and the quality of patients' lives improved if vaccines can activate immune responses against Cnm.

## Supplementary Material

Supplementary data is available at *Clinical and Experimental Immunology* online.

## Acknowledgments

We would like to thank Editage ([www.editage.com](http://www.editage.com)) for English language editing.

## Ethical Approval

The experimental protocol used in this study was approved by the Animal Care Committee of Hiroshima University (A18-112) and the epidemiological research ethics review committee of Hiroshima University (E-786-2). The animal research adheres to the ARRIVE guidelines (<https://arriveguidelines.org/arriveguidelines>).

## Conflict of Interests

The authors have no competing interests to declare.

## Funding

This research was supported by a Grant-in-Aid for Early-Career Scientists (21K16968), a Grant-in-Aid for Scientific Research (B) (21H03120), and a Grant-in-Aid for Scientific Research (C) (18K09599, 20K099405) from the Japan Society for the Promotion of Science.

## Author Contributions

Yuri Taniguchi: Data Curation, Investigation; Kazuhisa Ouhara: Conceptualization, Data Curation, Investigation, Funding acquisition, Writing - Original Draft; Masae Kitagawa: Conceptualization, Funding acquisition, Resources; Keiichi Akutagawa: Investigation; Miki Kawada-Matsuo: Methodology, Data Curation; Tetsuya Tamura: Investigation; Ruoqi Zhai: Investigation; Yuta Hamamoto: Formal analysis; Mikihito Kajiya: Validation, Writing - Review & Editing; Shinji Matsuda: Visualization; Hirofumi Maruyama: Supervision; Hitoshi Komatsuzawa: Methodology; Hideki Shiba: Validation, Funding, Writing - Review & Editing; Noriyoshi Mizuno: Supervision

## Data Availability

All data generated or analyzed during this study are included in the published article.

## Permission to Reproduce (for relevant content)

The datasets used and/or analyzed during the current study are available from the corresponding author on reasonable request.

## Clinical Trial Registration

None.

## References

1. Popa-Wagner A, Dumitrascu DI, Capitanescu B, Petcu EB, Surugiu R, Fang WH, et al. Dietary habits, lifestyle factors and neurodegenerative diseases. *Neural Regen Res* 2020, 15, 394–400. doi:10.4103/1673-5374.266045.
2. Lackland DT, Roccella EJ, Deutsch AF, Fornage M, George MG, Howard G, et al.; American Heart Association Stroke Council. Factors influencing the decline in stroke mortality: a statement from the American Heart Association/American Stroke Association. *Stroke* 2014, 45, 315–53. doi:10.1161/01.str.0000437068.30550.cf.
3. Sommer CJ. Ischemic stroke: experimental models and reality. *Acta Neuropathol* 2017, 133, 245–61. doi:10.1007/s00401-017-1667-0.
4. Boehme AK, Esenwa C, Elkind MS. Stroke risk factors, genetics, and prevention. *Circ Res* 2017, 120, 472–95. doi:10.1161/CIRCRESAHA.116.308398.
5. Donnan GA, Fisher M, Macleod M, Davis SM. Stroke. *Lancet* 2008, 371, 1612–23. doi:10.1016/S0140-6736(08)60694-7.
6. Broderick J, Connolly S, Feldmann E, Hanley D, Kase C, Krieger D, et al.; American Heart Association. Guidelines for the management of spontaneous intracerebral hemorrhage in adults: 2007 update: a guideline from the American Heart Association/American Stroke Association Stroke Council, High Blood Pressure Research Council, and the Quality of Care and Outcomes in Research Interdisciplinary Working Group. *Stroke* 2007, 38, 2001–23. doi:10.1161/STROKEAHA.107.183689.
7. Woo D, Sauerbeck LR, Kissela BM, Khoury JC, Szaflarski JP, Gebel J, et al. Genetic and environmental risk factors for intracerebral hemorrhage: Preliminary results of a population-based study. *Stroke* 2002, 33, 1190–5. doi:10.1161/01.str.0000014774.88027.22.
8. Hajishengallis G. Immunomicrobial pathogenesis of periodontitis: keystones, pathobionts, and host response. *Trends Immunol* 2014, 35, 3–11. doi:10.1016/j.it.2013.09.001.
9. Hajishengallis G. Periodontitis: From microbial immune subversion to systemic inflammation. *Nat Rev Immunol* 2015, 15, 30–44. doi:10.1038/nri3785.
10. Bordagaray MJ, Fernandez A, Garrido M, Astorga J, Hoare A, Hernandez M. Systemic and extraradicular bacterial translocation in apical periodontitis. *Front Cell Infect Microbiol* 2021, 11, 649925. doi:10.3389/fcimb.2021.649925.
11. Sato Y, Okamoto K, Kagami A, Yamamoto Y, Igarashi T, Kizaki H. *Streptococcus mutans* strains harboring collagen-binding adhesin. *J Dent Res* 2004, 83, 534–9. doi:10.1177/154405910408300705.
12. Nomura R, Nakano K, Taniguchi N, Lapirattanakul J, Nemoto H, Gronroos L, et al. Molecular and clinical analyses of the gene encoding the collagen-binding adhesin of *Streptococcus mutans*. *J Med Microbiol* 2009, 58, 469–75. doi:10.1099/jmm.0.007559-0.
13. Nakano K, Hokamura K, Taniguchi N, Wada K, Kudo C, Nomura R, et al. The collagen-binding protein of *Streptococcus mutans* is involved in haemorrhagic stroke. *Nat Commun* 2011, 2, 485. doi:10.1038/ncomms1491.
14. Hosoki S, Saito S, Tonomura S, Ishiyama H, Yoshimoto T, Ikeda S, et al. Oral carriage of *Streptococcus mutans* harboring the cnm gene relates to an increased incidence of cerebral microbleeds. *Stroke* 2020, 51, 3632–9. doi:10.1161/STROKEAHA.120.029607.
15. Kawada-Matsuo M, Oogai Y, Zendo T, Nagao J, Shibata Y, Yamashita Y, et al. Involvement of the novel two-component NsrRS and LcrRS systems in distinct resistance pathways against nisin A and nukacin ISK-1 in *Streptococcus mutans*. *Appl Environ Microbiol* 2013, 79, 4751–5. doi:10.1128/AEM.00780-13.
16. Kitagawa M, Nagamine K, Oka H, Ouhara K, Ogawa I, Komatsuzawa H, et al. Rapid detection of the *Streptococcus*

- mutans* *cnm* gene by loop-mediated isothermal amplification. *Anal Biochem* 2020, 605, 113812. doi:10.1016/j.ab.2020.113812.
17. Furusho H, Miyauchi M, Hyogo H, Inubushi T, Ao M, Ouhara K, et al. Dental infection of *Porphyromonas gingivalis* exacerbates high fat diet-induced steatohepatitis in mice. *J Gastroenterol* 2013, 48, 1259–70. doi:10.1007/s00535-012-0738-1.
  18. Naito Y, Nagata T, Takano Y, Nagatsu T, Ohara N. Rapeseed oil ingestion and exacerbation of hypertension-related conditions in stroke prone spontaneously hypertensive rats. *Toxicology* 2003, 187, 205–16. doi:10.1016/s0300-483x(03)00052-0.
  19. Munenaga S, Ouhara K, Hamamoto Y, Kajiya M, Takeda K, Yamasaki S, et al. The involvement of C5a in the progression of experimental arthritis with *Porphyromonas gingivalis* infection in SKG mice. *Arthritis Res Ther* 2018, 20, 247. doi:10.1186/s13075-018-1744-3.
  20. Takamatsu H, Tatsumi M, Nitta S, Ichise R, Muramatsu K, Iida M, et al. Time courses of progress to the chronic stage of middle cerebral artery occlusion models in rats. *Exp Brain Res* 2002, 146, 95–102. doi:10.1007/s00221-002-1147-0.
  21. Kawai T, Paster BJ, Komatsuzawa H, Ernst CW, Goncalves RB, Sasaki H, et al. Cross-reactive adaptive immune response to oral commensal bacteria results in an induction of receptor activator of nuclear factor-kappaB ligand (RANKL)-dependent periodontal bone resorption in a mouse model. *Oral Microbiol Immunol* 2007, 22, 208–15. doi:10.1111/j.1399-302X.2007.00348.x.
  22. Ouhara K, Munenaga S, Kajiya M, Takeda K, Matsuda S, Sato Y, et al. The induced RNA-binding protein, HuR, targets 3'-UTR region of IL-6 mRNA and enhances its stabilization in periodontitis. *Clin Exp Immunol* 2018, 192, 325–36. doi:10.1111/cei.13110.
  23. Asakawa R, Komatsuzawa H, Kawai T, Yamada S, Goncalves RB, Izumi S, et al. Outer membrane protein 100, a versatile virulence factor of *Actinobacillus actinomycetemcomitans*. *Mol Microbiol* 2003, 50, 1125–39. doi:10.1046/j.1365-2958.2003.03748.x.
  24. Johanson CE, Stopa EG, McMillan PN. The blood-cerebrospinal fluid barrier: structure and functional significance. *Methods Mol Biol* 2011, 686, 101–31. doi:10.1007/978-1-60761-938-3\_4.
  25. Lemos JA, Palmer SR, Zeng L, Wen ZT, Kajfasz JK, Freires IA, et al. The biology of *Streptococcus mutans*. *Microbiol Spectr* 2019, 7(1). doi:10.1128/microbiolspec.GPP3-0051-2018.
  26. Krzysciak W, Jurczak A, Koscielniak D, Bystrowska B, Skalniak A. The virulence of *Streptococcus mutans* and the ability to form biofilms. *Eur J Clin Microbiol Infect Dis* 2014, 33, 499–515.
  27. Matsumoto-Nakano M. Role of *Streptococcus mutans* surface proteins for biofilm formation. *Jpn Dent Sci Rev* 2018, 54, 22–9. doi:10.1016/j.jdsr.2017.08.002.
  28. Inenaga C, Hokamura K, Nakano K, Nomura R, Naka S, Ohashi T, et al. A potential new risk factor for stroke: *Streptococcus mutans* with collagen-binding protein. *World Neurosurg* 2018, 113, e77–81. doi:10.1016/j.wneu.2018.01.158.
  29. Miyatani F, Kuriyama N, Watanabe I, Nomura R, Nakano K, Matsui D, et al. Relationship between *Cnm*-positive *Streptococcus mutans* and cerebral microbleeds in humans. *Oral Dis* 2015, 21, 886–93. doi:10.1111/odi.12360.
  30. Nakano K, Tsuji M, Nishimura K, Nomura R, Ooshima T. Contribution of cell surface protein antigen PAc of *Streptococcus mutans* to bacteremia. *Microbes Infect* 2006, 8, 114–21. doi:10.1016/j.micinf.2005.06.005.
  31. Brady LJ, Maddocks SE, Larson MR, Forsgren N, Persson K, Deivanayagam CC, et al. The changing faces of *Streptococcus* antigen I/II polypeptide family adhesins. *Mol Microbiol* 2010, 77, 276–86. doi:10.1111/j.1365-2958.2010.07212.x.
  32. Aviles-Reyes A, Miller JH, Lemos JA, Abranches J. Collagen-binding proteins of *Streptococcus mutans* and related streptococci. *Mol Oral Microbiol* 2017, 32, 89–106. doi:10.1111/omi.12158.
  33. Al-Obaidi MMJ, Desa MNM. Mechanisms of blood brain barrier disruption by different types of bacteria, and bacterial-host interactions facilitate the bacterial pathogen invading the brain. *Cell Mol Neurobiol* 2018 Oct, 38, 1349–68. doi:10.1007/s10571-018-0609-2.
  34. Wimmer I, Tietz S, Nishihara H, Deutsch U, Sallusto F, Gosselet F, et al. PECAM-1 stabilizes blood-brain barrier integrity and favors paracellular T-cell diapedesis across the blood-brain barrier during neuroinflammation. *Front Immunol* 2019 Apr 5, 10, 711. doi:10.3389/fimmu.2019.00711.
  35. Tasaka S, Qin L, Saijo A, Albelda SM, DeLisser HM, Doerschuk CM. Platelet endothelial cell adhesion molecule-1 in neutrophil emigration during acute bacterial pneumonia in mice and rats. *Am J Respir Crit Care Med* 2003 Jan 15, 167, 164–70. doi:10.1164/rccm.2202011.